CFD STUDY OF THE SINGLE-PHASE SUBCHANNEL TURBULENT MIXING IN TIGHT LATTICE GEOMETRY WITH IMPROVED WALL TREATMENT

M. Liu, Y. Ishiwatari
The University of Tokyo, Tokyo, Japan

Abstract

This paper focuses on the numerical simulation of turbulence mixing phenomena in tight lattice geometries. The use of RANS for mixing phenomenon has been carried out. For large *P*/*D* subchannels, the influence of anisotropic of turbulence is not significant, and mixing rate between subchannels is dominated by turbulence eddy diffusion. The comparison between numerical results and experimental results proves that acceptable accuracy can be achieved for the mixing coefficient by steady-state and transient calculation with RANS models. However, for smaller *P*/*D* geometries, because of the strong anisotropy in the gap region, the contribution of macroscopic pulsation to mixing rate cannot be neglected any more, proved that the mixing rate is dramatically enhanced by the flow pulsation. Transient calculation with anisotropic turbulence model would be necessary.

1. Introduction

The prediction of the detailed temperature distribution of rod bundles, used especially as nuclear fuel elements, is required to ensure their safe and reliable operation. In nuclear reactors, the turbulent mixing is a significant physical phenomenon that strongly influences the velocity and temperature distribution inside rod-bundles [1]. The study of the phenomena that rule turbulent mixing has been motivating many works and experiments since the early days of nuclear power reactors [2].

As the core coolant flow rate per thermal power of the SCWRs is much smaller than that of LWRs, the fuel bundle geometry of the SCWRs is tight lattice where the pitch (*P*) to diameter (*D*) ratio *P*/*D* is below 1.2 in order to keep high mass flux for heat removal. The conceptual design studies on the SCWRs at the Univ. Tokyo have shown that subchannel analyses are essential for thermal hydraulic design and safety analysis in order to avoid significant under-estimation of maximum cladding surface temperature (MCST) [3]. Importance of the turbulent mixing is higher in the SCWRs than the LWRs because the cross flow driven by pressure distribution is relatively weak in the SCWRs with narrow gap. In the subchannel analysis codes, the turbulent mixing between neighboring subchannels are calculated by using the turbulent mixing coefficient that is empirically given. As there are no experimental data of turbulent mixing coefficient under tight lattice and supercritical-pressure condition, the data for subcritical-pressure single-phase condition in tight lattice is temporality applied [3, 4]. The recent sensitivity analysis implies that the MCST is very sensitive to the turbulent mixing coefficient [4]. Thus, among various R&D items on the SCWR thermal-hydraulics, high priority should be given to determination of the turbulent mixing coefficient for improving the subchannel analysis code. Kyushu Univ. is planning to measure the turbulent mixing coefficient of supercritical-fluid for the first time under the research program “Research and development of Super Fast Reactor (phase-II)” [5]. That experimental data will be very helpful for validating numerical simulations. As the first step of predicting the mixing coefficient in the SCWR conditions, this study aims at predicting it by CFD in tight lattice geometry under subcritical-pressure single-phase condition.

Despite the achievement of turbulent modeling and numerical simulation, traditional CFD fails to accurately predict distributions of velocity, temperature and wall shear stresses when the *P*/*D* is smaller than a threshold value (i.e., 1.1 for triangular lattices of cylindrical pins) as reported by Krauss and Meyer [6]. For the flow in tight lattice geometry like SCWRs, both experiments and Direct Numerical Simulation (DNS) have clearly revealed that flow conditions inside fuel bundles are very different from those of typical pipe flow due to strong anisotropy in the non-uniform channel geometry [7]. At a long time, the high mixing rate was attributed to the secondary flow [8] since the mixing rates measured by experiments were higher than those could be accounted for by turbulent diffusion along [9]. An important observation was reported in 1970 by van der Ros and Bogaardt [10] that there are very regular pulsation in amplitude and frequency in the gap. In 1972, the experimental results of Rowe et al.[11, 12] show that there exists an additional macroscopic flow process in the regions adjacent to the gaps, i.e. large scale turbulence moves through the gaps which can be considered as a periodic flow pulsation across the gap, which was considered as an additional important part for the high mixing rate.

The accuracy of the turbulent mixing calculation is dominated by the anisotropy of turbulence flow in the narrow region. Early investigations tried to calculate turbulent mixing on the basis of isotropic turbulence, resulting in significant under-estimation of the mixing values compared to the experiments [2]. Also in the fully developed turbulent flows in a fuel pin subassembly without spacer effects, there are a couple of interesting phenomena that were hardly captured in the past by the Reynolds-Averaged Navier-Stokes (RANS) equations approach with isotropic k-ε turbulence models but found theoretically or experimentally, as they are connected to the anisotropy of turbulence [13]. In order to develop a methodology capable of modeling flow inside tight lattice fuel bundles, preliminary comparisons and evaluations have already been done by the many researchers, both for isothermal cases and for heated rod bundles. A wide variety of models were investigated, to show their limitations and advantages. Ninokata[13] focuses on the numerical simulation of low Reynolds (Re) number turbulence flow phenomena in tightly packed fuel pin subassemblies and in channels of irregular shape by DNS, Large Eddy Simulation (LES) and RANS equations approach. They found that complicated turbulent flow structure in subchannels is due to strong anisotropy in the non-uniform channel geometry that is characterized by wide open channels connected by a narrow gap. The secondary flows in subchannels play an important role in transporting small eddies generated in the wider region toward the narrow gap. Periodic cross-flow oscillations are calculated to appear in the vicinity of the gap region, and the coherent structure is transported in the main flow direction.

Among many approaches of CFD, DNS is the most preferred when we try to investigate the phenomena whose mechanisms are unknown or not clearly understood [14]. However, it is well understood that simulating a whole bundle by DNS is not possible, while it could be done by LES on high-end computers available. Thus the purpose of this work is to validate the current turbulent model(s) and numerical method(s) for the turbulent mixing calculation, and try to modify or develop some engineering applicable model(s) or method(s) that can accurately capture the turbulent flow phenomena in tight lattice geometry, and apply them to nuclear reactor thermo-hydraulic design and safety analysis.

2. Subchannel calculations

2.1 Model description

The *k-ω* Shear Stress Transport (SST) model [15] which in stead of the dissipation rate, *ε*, adopt an equation for the turbulent frequency, *ω*, of the large scales. For *k-ω* SST model, the general form of the *k* and *ω* equation is as follows:

$$\frac{\partial(\rho k)}{\partial t}+\frac{\partial(\rho U_i k)}{\partial x_i}-\frac{\partial}{\partial x_i}\left[(\mu+\sigma_k\mu_t)\frac{\partial k}{\partial x_i}\right]=\widetilde{P_k}-\beta\rho k\omega \tag{1}$$

$$\frac{\partial(\rho\omega)}{\partial t}+\frac{\partial(\rho U_i \omega)}{\partial x_i}-\frac{\partial}{\partial x_i}\left[(\mu+\sigma_\omega\mu_t)\frac{\partial \omega}{\partial x_i}\right]=\frac{\alpha}{\nu_t}k\widetilde{P_k}-\beta\rho\omega^2 + 2(1-F_1)\rho\sigma_{\omega 2}\frac{1}{\omega}\frac{\partial k}{\partial x_i}\frac{\partial \omega}{\partial x_i} \tag{2}$$

$$\nu_t=\frac{a_1 k}{\max(a_1\omega, SF_2)};\qquad S=\sqrt{2S_{ij}S_{ij}} \tag{3}$$

$$P_k=\mu_t\frac{\partial U_i}{\partial x_j}\left(\frac{\partial U_i}{\partial x_j}+\frac{\partial U_j}{\partial x_i}\right);\qquad \widetilde{P_k}=\min(P_k, 10\beta k\omega) \tag{4}$$

$$F_1=\tanh\left\{\left\{\min\left[\max\left(\frac{\sqrt{k}}{\beta\omega y},\frac{500\nu}{\omega y^2}\right),\frac{\sqrt{k}}{CD_{k\omega}y^2}\right]\right\}^4\right\}$$
$$F_2=\tanh\left\{\left[\max\left(\frac{2\sqrt{k}}{\beta\omega y},\frac{500\nu}{\omega y^2}\right)\right]^2\right\} \tag{5}$$

$$CD_{k\omega}=\max\left(2\rho\sigma_{\omega 2}\frac{1}{\omega}\frac{\partial k}{\partial x_i}\frac{\partial \omega}{\partial x_i},10^{-10}\right) \tag{6}$$

where *k* is the turbulence kinetic energy, *ω* is the turbulence frequency, *y* is the distance to the nearest wall, S is the invariant measure of the strain rate, *ρ* is the density and U_i is the flow velocity. F_1 and F_2 are blending functions which are equal to zero away from the surface (*k-ε* model), and switches over to inside to the boundary layer (*k-ω* model) [16]. All constants are computed by a blend from the corresponding constants of the *k-ε* and the *k-ω* model via $\alpha = \alpha_1 F_1 + \alpha_2(1-F_1)$, etc. the constants for this model are $\beta = 0.09$, $\alpha_1=5/9$, $\beta_1=3/40$, $\sigma_{k1}=0.95$, $\sigma_{\omega 1}=0.5$, $\alpha_2=0.44$, $\beta_2=0.0828$, $\sigma_{k2}=1$, $\sigma_{\omega 1}=0.856$.

2.2 Compound wall treatment

The near wall treatment is of equal importance in practical industrial CFD simulations as the formulation of the turbulence model itself [16]. The continuous increase in computing power has resulted- among others- in a trend towards using denser computational grids for computing industrial flows. However, because of prohibitive costs, in most cases such grids are still too coarse to satisfy the prerequisites for the Integrate to Wall (ItW). Instead, the first grid point often lies in the buffer layer ($5 \le y^+ < 30$ in the wall attached flows), making neither ItW nor WF applicable [17]. Recently, several proposals appeared in the literature aimed at improving and generalising the wall treatment.

One can distinguish two approaches. The first approach, based on early ideas of Chieng and Launder [18] pursues to derive wall functions by splitting the first near-wall cell into a viscosity-affected sublayer and the fully turbulent part, then assuming the variation of all flow properties in each part of the cell and integrating the expressions over the complete cell. A more general variant of such an approach are the so called Analytical Wall Functions of Craft et al [19]. The second approach employs a blending between the wall-limiting and fully turbulent expressions for various flow properties in question, using blending functions that ensure a smooth transition between the two layers. This makes it possible to provide adequate conditions for the first near-wall grid node even if it lies in the buffer region [17]. M. Popovac and K. Hanjalic presented compound wall treatment (CWT), which reduces either to the ItW when the first near-wall cell is in the viscous sublayer, or to the appropriate WF when it lies in the fully turbulent region. When the first grid node is in the buffer region, the boundary conditions are provided from blending the viscous and fully turbulent limits using exponential blending functions.

2.3 Mass transfer

In order to model the mixing in the subchannels, additional equations is solved for the concentration *c*. The transport equation for the passive scalar *c* can be written as:

$$\frac{\partial C}{\partial t}+\frac{\partial\left(U_i C\right)}{\partial x_i}=\frac{\partial}{\partial x_i}\left[D_{ab}\frac{\partial C}{\partial x_i}+\overline{u_i c_i}\right] \tag{7}$$

$$\overline{u_i c_i}=\frac{\nu_t}{Sc_t}\frac{\partial C}{\partial x_i} \tag{8}$$

where D_{ab} is the molecular diffusivity of the tracer fluid, and Sc_t is the turbulent Schmidt number. Turbulent Schmidt number is of the order of unity, values in the literature varying from 0.5 to 1. For flow in jets and wakes the value is more nearly 0.5 [20]. In this work we choose the value 0.5.

2.4 Model validation

A series of velocity and wall shear stress measurements, that were performed by Mantlik et al. are adopted by Baglietto and Ninokata as benchmark. The experiments were completed in a wind tunnel, using a 19 rods model with triangular array configuration and an outer diameter of 120mm simulating a fuel assembly. The *P*/*D* ratio is 1.17. Length of the model was 6 m and the measurements were performed inside the model at a distance of 5600mm from the model inlet, i.e. in the region of fully developed turbulent flow and without the back effect of outlet cross-section change. The measurements were performed in a central subchannel, so that it can be considered an elementary flow cell of an infinite rod bundle. The Reynolds number, based on bulk velocity and bundle hydraulic diameter, considered in this case is 64,300.

When simulating an infinite triangularly arrayed rod bundle of cylindrical pins, under fully developed flow conditions, due to the symmetry it is sufficient to simulate only one sixth of a subchannel, adopting the appropriate symmetric boundaries, which constitutes an elementary infinite flow cell as shown in Figure 1. In the axial direction, due to the fully developed conditions, it is possible to apply cyclic boundaries between inlet and outlet, while fixing the inlet mass flow rate as

input. The height of the computational model can be therefore extremely reduced without interfering with the correctness of the calculation; in this case a height of 20 mm is adopted.

Computational results based on the previously described turbulence models have been compared with the experimental data available. The wall shear stress distribution by Krauss and Meyer [6], normalised by the average shear for the 0 to 30° segment, is shown by Figure 2. For comparison, a numerically prediction by CFD calculation for an infinite subchennels was also presented. Baglietto and Ninokata [21] already shown that the *k-ε* as well as the SST and SST with compound wall treatment (SST_CWT) produce very similar predictions, where the wall shear stress monotonically increase toward the center of the subchannel.

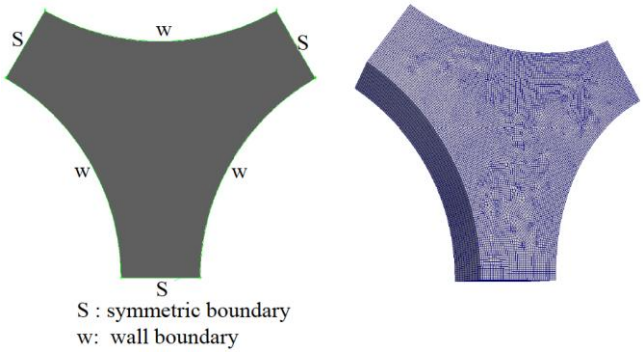

Figure 1 Subchannel and adopted calculation grids

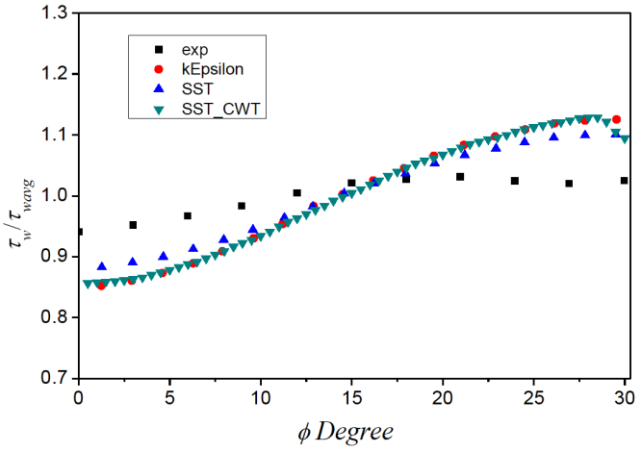

Figure 2 Wall shear stress for Re=64,300 [21]

3. Turbulent mixing calculation

3.1 Experiment used for validation

In order to investigate the problem experimentally, a turbulent mixing experiment under single-phase, fully developed flow conditions without pressure difference in a two-channel experiment carried out by Kumamoto University, Japan[22]. Single-phase turbulent mixing rate was obtained using a tracer technique under adiabatic conditions with three test channels, as shown in Figure 3. In Ch. F-F, two identical circular subchannels of 16.0 mm are interconnected through a gap. The turbulent mixing rate between the subchannels was measured by a tracer technique for fully developed turbulent flows of water (or air) at atmospheric pressure and at room temperature using acid orange II solution (or methane) as the tracer fluid. In order to produce fully developed flow at the inlet of the mixing section, the length of the entry section was set to 2.0 m, and the length of the mixing and outlet section were 2.5 m and 0.5 m respectively. The range of Reynolds number covers was 5800-66400. The experiment uncertainties of the water mixing rate and the air mixing rate in the experiment were evaluated to be 6% and 8% respectively [22]. As the axial distribution of the tracer concentration in both subchannels were measured, the turbulent mixing rate *w'* was obtained as

$$\frac{C_i(Z+\Delta Z)-C_j(Z+\Delta Z)}{C_i(Z)-C_j(Z)}=\exp\left(-\Delta Z\frac{G_iA_i+G_jA_j}{G_iA_iG_jA_j}w'\right) \quad (9)$$

where G_i and A_i are the mass flux and the cross-section area of a subchannel I, $C_i(Z)$ is the tracer concentration in the subchannel i at an axial position Z, and ΔZ is the distance between two axial position.

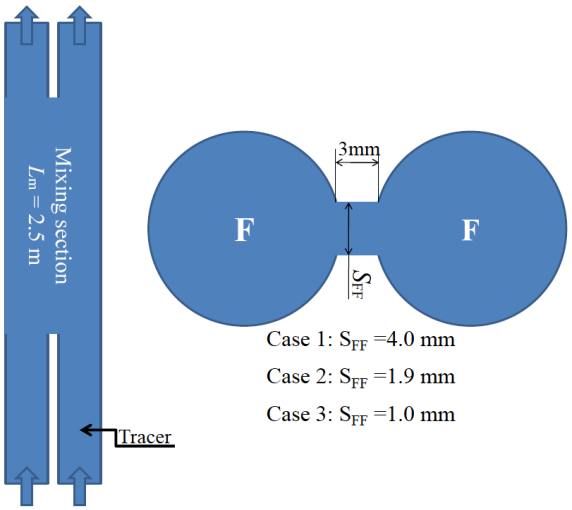

Figure 3 Cross-section of the test section

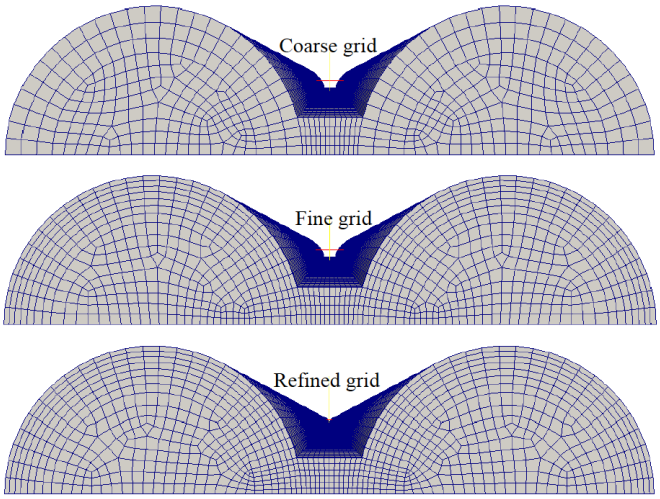

Figure 4 Adopted calculation grids

3.2 Turbulence mixing calculation

Due to the symmetry of the flow channel, it is sufficient to simulate only half of the channel. In the axial direction, due to the fully developed conditions, it is possible to apply cyclic boundaries between inlet and outlet, while fixing the inlet mass flow rate and the inlet tracer concentration as input. The height of the computational model can be mainly concentrated on the mixing section as the inlet and outlet section was reduced to 160mm ($10\times D_h$), therefore extremely reduced without interfering with the correctness of the calculation. It is straightforward that the importance of the "numerical viscosity" is directly proportional to the grid size and to the discretization scheme order [21]. In our approach, repeating the calculations on different finesse grids and with different numerical schemes allows to accurately evaluate the significance of the numerical smearing. Figure 4 shows the increasing grid finesses adopted for this case. The number of nodes for each grid and the dimensionless wall distance y^+ values for the near wall cells are given in the following Table 1.

Calculations are repeated on the three different grids adopting the Upwind scheme (UD) and linear Upwind scheme. The comparison shows that for flow field, the two finest grids are clearly converged, the results in fact do not present any distinguishable difference between the two cases and with both discretization schemes. Such convergence is appreciated by comparing the predictions for the maximum velocity inside the channel in each case, as given in Table 2. Also for the turbulent mixing rate, the difference between calculation results and the experiment results are within the maximum experiment error range 6%.

Table 1 Calculation grids date

Model	Number of nodes	Averaged y^+ value at the near wall cell (Re = 29,300)
Coarse grid	1,018,140	46.732
Fine grid	1,652,176	18.800
Refined grid	1,942,580	16.801

Table 2 Calculated turbulent mixing coefficient

Model	Maximum Velocity	Difference	Turbulence mixing rate	Difference with the experiment
Coarse grid (UD)	1.79	-1.97%	28.10	+5.71%
Coarse grid (linear UD)	1.79	-1.97%	28.11	+5.68%
Fine grid (UD)	1.83	0	27.03	+5.46%
Fine grid (linear UD)	1.83	0	27.04	+5.42%
Refined grid (UD)	1.83	0	29.94	+4.76%
Refined grid (linear UD)	1.83	0	29.95	+4.75%

4. Results and discussion

Because of the importance of the mixing coefficients for the design of nuclear fuel element many experiments and simulation work have been done to study the surprisingly high mixing rate between subchannels. The coolant mixing could be explained in general by several transport mechanisms, e.g., convection by divergence cross-flow, turbulence and molecular diffusion, and other macroscopic flow processes including the global flow pulsation[13].

4.1 Molecular and turbulent diffusion

Molecular and turbulence diffusion, especially the latter one, is considered as the important driven force for mass transfer. For large *P*/*D* subchannel flow, turbulence diffusion does play an important role on mixing rate. However, for small gap subchannel flow, because of the existence of a special phenomena--turbulence to laminar transition, the influence of turbulence diffusion on mixing rate in the gap region is much waker. DNS calculation for the low bulk *Re* numbers (Re_{bulk}) have shown that a turbulent region is developing into the narrow gap region as Re_{bulk} increase but there still remains a locally laminar flow in the gap region [13]. For all the cases of current calculation, the average boundary layer thickness is around 0.0065 m, much larger than the gap size. Figure 5 shows the distribution of the maximum dimensionless turbulent viscosity μ_t^+ in the 4 mm gap region. For large gap cases (S_{FF} = 4mm), turbulence eddy diffusion play an important role on the mixing rate, thus steady-state calculation can get good results although the contribution of macroscopic pulsation is ignored.

4.2 Macroscopic flow pulsation

The macroscopic flow pulsations is considered as an additional effect to enhance the mixing through the gap of rod bundles [9]. The macroscopic flow pulsations observed by Rowe [11, 12] have been confirmed and stressed by Hooper [23], Hooper and Rehme [24], and Renksizbulut and Hadaller [25]. These instabilities were found in subchannels connected by narrow gaps or pitch to diameter (*P*/*D*). Lack of modeling of the flow pulsation has been pointed out to be one of the reasons for this underestimation as discussed in Krauss and Meyer [6]. As the substantial failure of steady-state RANS model on capturing these instabilities, transient calculation with nonlinear turbulence models [21] as well as Explicit Algebraic Reynolds Stress Model (EARSM) [26] were carried out for the small gap cases. The cross velocity in each narrow gap has a quasi-sinusoidal behavior and a power spectrum with a peak frequency, which is quite different with the spectrum of homogeneous turbulence [1]. This is also confirmed by current calculation as shown in Figure 6. For extremely tight lattice geometry, the flow in the gap region is deep in the boundary layer, the influence of

turbulent eddy diffusion on mixing rate is quite wake, so the existence of large-scale periodic flow oscillations is responsible for the high mixing rate [27]. Also compare case (a) and (b) in Figure 7, both the peak and averaged intensity of the pulsation decrease with the increase of the gap size because the turbulence would be more isotropic. The detailed discussion of this coherent structure as well as its influence on the turbulent mixing rate will be done in the future work.

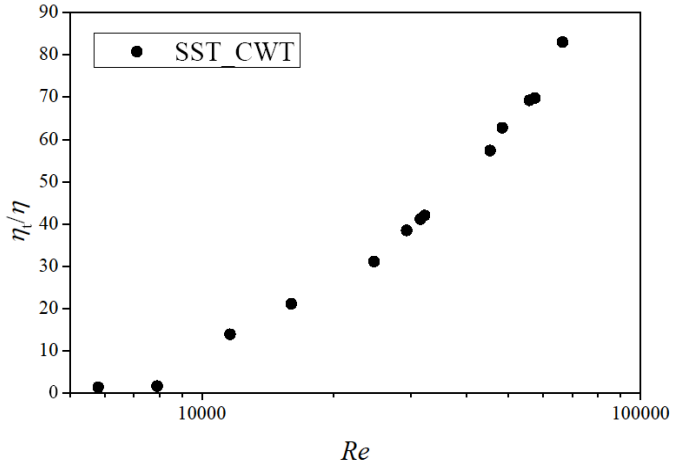

Figure 5 Turbulent viscosity ratio

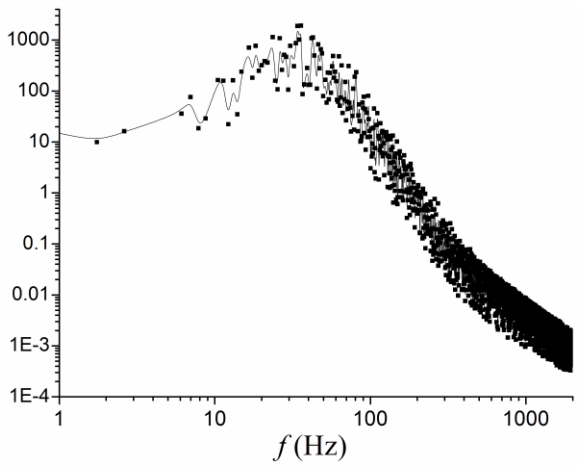

Figure 6 Power spectrum of pulsation velocity in the center of gap

4.3 Secondary flow

Another important feature of the flow in rod bundles is the presence of Reynolds-averaged secondary flow in the cross section [1]. Although at early times the high mixing rate between subchannels was explained by secondary flow [9]. However, later experiments and numerical simulation showed that secondary flow cannot be the reason for high mixing rates measured for low-gap-to-diameter ratios [9]. Because the secondary flow velocities are very small. It is obvious that secondary flow do not contribute significantly to the mixing between subchannels of rod bundles since the secondary flow vortices are expected to move within the elementary cells of the subchannels. They do not cross the gaps between the subchannels. In general, the secondary flow vorticity concentrates in the vicinity of the pin walls as P/D decrease, and the turbulence anisotropy is enhanced in the gap region. Figure 7 (2) shows the time-averaged secondary flow distribution for three cases with different gap size by transient calculation with EARSM model. The secondary flow is much smaller than the pulsation velocity across the gap, and it does not cross the gap.

4.4 Turbulent mixing calculation results

For large gap size cases (4mm case), the turbulent mixing was calculated with steady state calculation at 4 mm gap case, where the contribution of the coherent structure is not significant. Figure 8 shows the tracer fluid concentration distribution along the subchannel *i* and *j* due to turbulent mixing and molecular diffusion. However, the molecular diffusivity between water and acid orange II is nearly 10^{-9}, so the mass transfer is mainly due to turbulent mixing.

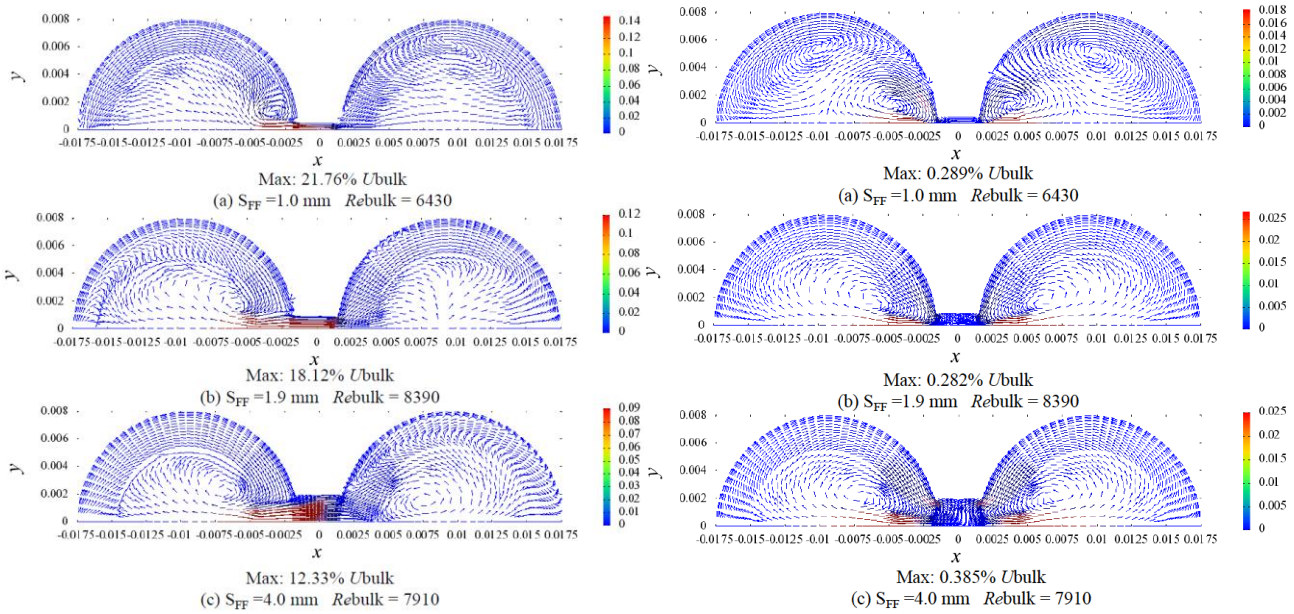

(1) Instantaneous vector plot (2) Time averaged velocity

Figure 7 Secondary flow

High Reynolds number version RANS model use empirical wall functions, to bridge the gap between the solid wall boundary and the turbulent core. However, the universality of such functions breaks down for complex flows. Figure 9 compares the performance of 3 types of frequently used *k*-*ε* models (including stand *k*-*ε* model, Realizable *k*-*ε* models as well as RNG *k*-*ε* model). The calculation results of these three models are little bit different, but all of them under-estimated the mixing rate about 50%. As the performance of *k*-*ε* models are quite similar, Figure 10 only shows the calculation results of water-acid orange II mixing cases by SST_CWT and standard *k*-*ε* models. The turbulence mixing rate is under-estimated against the experiment results by about 50%, while SST_CWT model has better performance compare to *k*-*ε* model. It can successfully reproduce all the 6 cases of water-acid orange II mixing. As already proved that stand *k*-*ε* models can not reproduce the experiment results, only the SST_CWT model was used to calculate the rest of the 6 cases of air-methane mixing. Figure 11 shows the mixing rate calculation results with only SST_CWT model of both water-acid orange II mixing cases and air-methane mixing cases. The calculation slightly under-estimated the mixing coefficient, however, if take the error of the experiment into consideration, the calculation results are quite close to the experiment. Also because of the steady-state calculation, the contribution of macroscopic pulsation to the mixing rate is ignored. It is clearly seen that the mixing coefficient depends strongly on mass flux [28].

However, for smaller *P*/*D* subchannels (with 1.0 mm or 1.9 mm), because of the anisotropic in the gap region, the contribution of macroscopic pulsation to mixing cannot be neglect any more, transient simulation with low *Re* number EARSM model are carried out to reflect the influence of anisotropic turbulence. Because of the computation domain is quite large, low Re number transient calculation is really time consuming for mass transfer calculation. Presently only three cases (one for each geometry) has been carried out. These three cases present coherent, turbulent structures in the narrow gap, which affects the distribution of the tracer concentration as well as they introduce turbulent mixing between subchannels, as shown in Figure 12. The calculation results proved that mixing rate is dramatically enhanced by the flow pulsation, and all these three cases can get good agreement of turbulent mixing rate compare with the experiment. Further study is going on for both flow field calculation and mass transfer calculation in narrow gap subchannels.

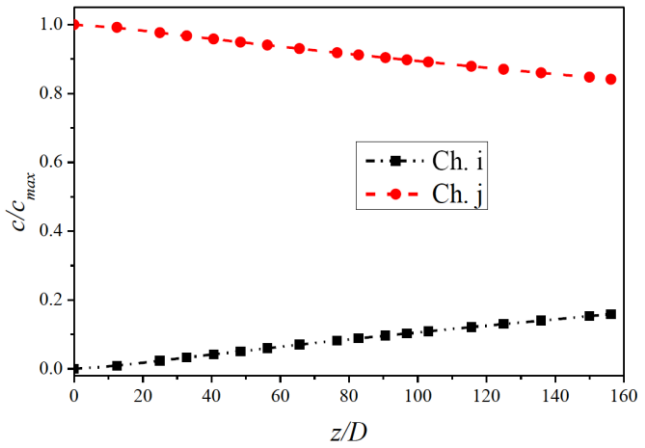

Figure 8 Tracer fluid concentration distribution along the subchannel *i* and *j* at Re = 57400

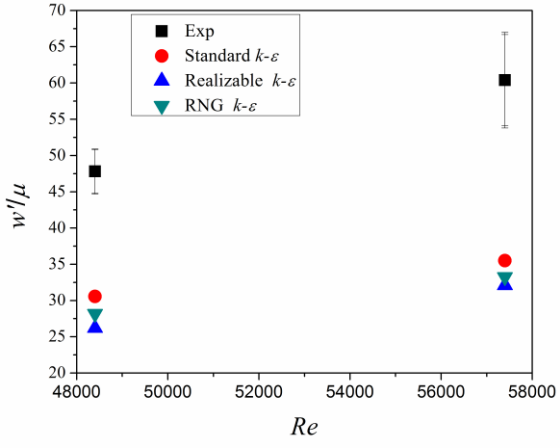

Figure 9 Turbulent mixing rate with three type of *k-ε* models

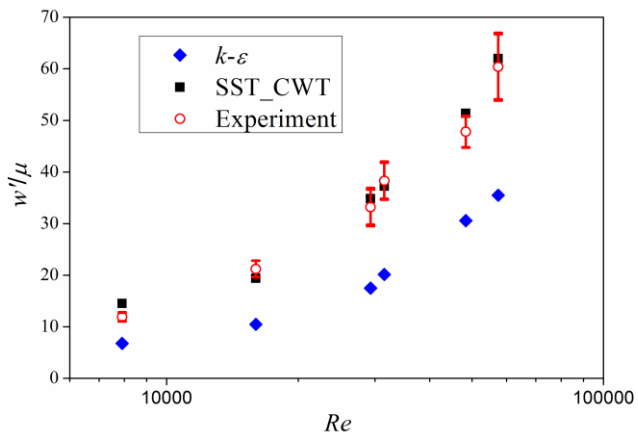

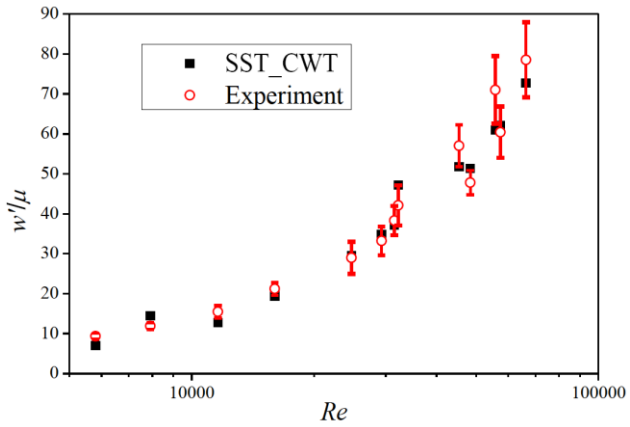

Figure 10 Turbulent mixing rate with difference turbulence model Figure 11 Turbulent mixing rate

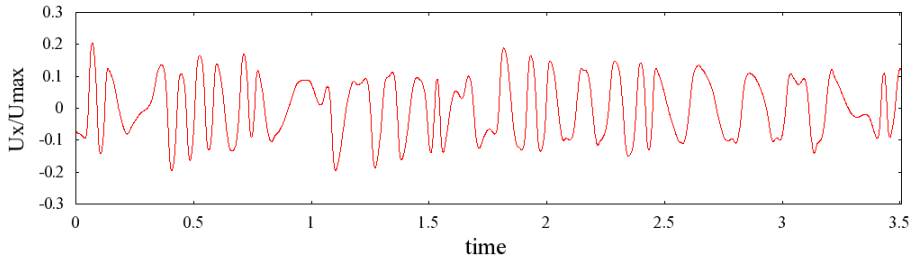

(a) Velocity component cross the gap

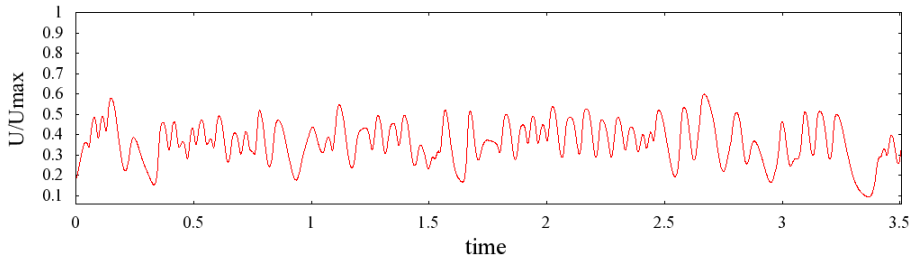

(b) Velocity

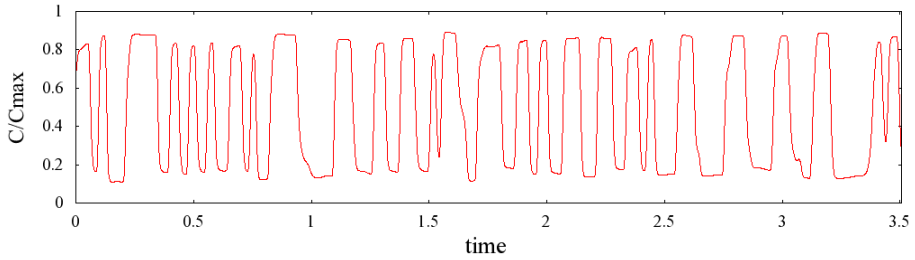

(c) Tracer concentration

Figure 12 Velocity and tracer concentration pulsation in the middle of the gap

5. Conclusion

As the first step of predicting the turbulent mixing coefficient in the SCWR bundle geometries, the flows in three different gap size subchannels have been simulated under subcritical-pressure single-phase condition through the use of RANS model. The case with 4mm gap, was carried out by steady-state SST_CWT turbulence model for mixing phenomenon. For this case, because of large *P*/*D*, the influence of anisotropic of turbulence is not significant, and mixing rate between subchannels is dominated by turbulence eddy diffusion. Steady-state calculation with SST model and CWT can successfully predict the mixing coefficient. However, for smaller *P*/*D* subchannels (with 1.0 mm or 1.9 mm), because of the anisotropic in the gap region, the contribution of macroscopic pulsation to mixing cannot be neglect any more, unsteady simulation with low Re number nonlinear k-ε as well as EARSM are carried out to show the influence of macroscopic flow pulsation on turbulent mixing. And calculation results proved that mixing rate is dramatically enhanced by the flow pulsation. Further study is needed on both flow field calculation and mass transfer calculation.

6. References

[1] E. Merzari, et al., "Unsteady Reynolds-averaged Navier-Stokes: toward accurate prediction of turbulent mixing phenomena", International Journal of Process Systems Engineering, Vol. 1, Iss. 1, 2009, pp. 100-123.

[2] N. Silin, L. Juanico, and D. Delmastro, "Thermal mixing between subchannels: measurement method and applications", Nuclear Engineering and Design, Vol. 227, Iss. 1, 2004, pp. 51-63.

[3] Y. Oka, et al., Super Light Water Reactors and Super Fast Reactors. 2010: Springer.

[4] Development of SCWR in GIF Collaboration (Phase-I). FY2008 and FY2009 annual reports.

[5] Y. Oka, RESEARCH AND DEVELOPMENT OF SUPER LIGHT WATER REACTORS AND SUPER FAST REACTORS IN JAPAN, in *In. Symp. on SCWR*. 2010: Vancouver, Canada.

[6] T. Krauss and L. Meyer, "Experimental investigation of turbulent transport of momentum and energy in a heated rod bundle", Nuclear Engineering and Design, Vol. 180, Iss. 3, 1998, pp. 185-206.

[7] H. Ninokata, et al., "Direct Numerical Simulation of Turbulent Flows in a Subchannel of Tight Lattice Fuel Pin Bundles of Nuclear Reactors", Annual Report of the Earth Simulator Center April, Vol. 2005, Iss., 2004.

[8] V. Skinner, A. Freeman, and H. Lyall, "Gas mixing in rod clusters", International Journal of Heat and Mass Transfer, Vol. 12, Iss. 3, 1969, pp. 265-278.

[9] K. Rehme, "The structure of turbulence in rod bundles and the implications on natural mixing between the subchannels", International Journal of Heat and Mass Transfer, Vol. 35, Iss. 2, 1992, pp. 567-581.

[10] T. Van der Ros and M. Bogaardt, "Mass and heat exchange between adjacent channels in liquid-cooled rod bundles", Nuclear Engineering and Design, Vol. 12, Iss. 2, 1970, pp. 259-268.

[11] D. Rowe, "Measurement of turbulent velocity, intensity and scale in rod bundle flow channels", Iss., 1973.

[12] D. Rowe and J. Johnson, "Implications concerning rod bundle crossflow mixing based on measurements of turbulent flow structure* 1", International Journal of Heat and Mass Transfer, Vol. 17, Iss. 3, 1974, pp. 407-419.

[13] H. Ninokata, E. Merzari, and A. Khakim, "Analysis of low Reynolds number turbulent flow phenomena in nuclear fuel pin subassemblies of tight lattice configuration", Nuclear Engineering and Design, Vol. 239, Iss. 5, 2009, pp. 855-866.

[14] E. Merzari, H. Ninokata, and E. Baglietto, "Numerical simulation of flows in tight-lattice fuel bundles", Nuclear Engineering and Design, Vol. 238, Iss. 7, 2008, pp. 1703-1719.

[15] F. Menter, "Two-equation eddy-viscosity turbulence models for engineering applications", AIAA journal, Vol. 32, Iss. 8, 1994, pp. 1598-1605.

[16] F. Menter, "Review of the shear-stress transport turbulence model experience from an industrial perspective", International Journal of Computational Fluid Dynamics, Vol. 23, Iss. 4, 2009, pp. 305-316.

[17] M. Popovac and K. Hanjalic, "Compound wall treatment for RANS computation of complex turbulent flows and heat transfer", Flow, Turbulence and Combustion, Vol. 78, Iss. 2, 2007, pp. 177-202.

[18] C. Chieng and B. Launder, "On the calculation of turbulent heat transport downstream from an abrupt pipe expansion", Numerical Heat Transfer, Part A: Applications, Vol. 3, Iss. 2, 1980, pp. 189-207.

[19] T. Craft, et al., "A new wall function strategy for complex turbulent flows", Numerical Heat Transfer, Part B: Fundamentals, Vol. 45, Iss. 4, 2004, pp. 301-318.

[20] R. Bird, W. Stewart, and E. Lightfoot, eds. "Transport Phenomena", 2nd ed. 2002, John Wiley & Sons, USA.

[21] E. Baglietto and H. Ninokata, "A turbulence model study for simulating flow inside tight lattice rod bundles", Nuclear Engineering and Design, Vol. 235, Iss. 7, 2005, pp. 773-784.

[22] M. Sadatomi, A. Kawahara, and Y. Sato, "Prediction of the single-phase turbulent mixing rate between two parallel subchannels using a subchannel geometry factor", Nuclear Engineering and Design, Vol. 162, Iss. 2, 1996, pp. 245-256.

[23] J. Hooper, "Developed single phase turbulent flow through a square-pitch rod cluster", Nuclear Engineering and Design, Vol. 60, Iss. 3, 1980, pp. 365-379.

[24] J. Hooper and K. Rehme, "Large-scale structural effects in developed turbulent flow through closely-spaced rod arrays", Journal of Fluid Mechanics, Vol. 145, Iss., 1984, pp. 305-337.

[25] G. Renksizbulut, "An experimental study of turbulent flow through a square-array rod bundle", Nuclear Engineering and Design, Vol. 91, Iss. 1, 1986, pp. 41-55.

[26] S. Wallin and A. Johansson, "An explicit algebraic Reynolds stress model for incompressible and compressible turbulent flows", Journal of Fluid Mechanics, Vol. 403, Iss., 2000, pp. 89-132.

[27] S. Möller, "On phenomena of turbulent flow through rod bundles", Experimental Thermal and Fluid Science, Vol. 4, Iss. 1, 1991, pp. 25-35.

[28] X. Cheng and U. Müller, "Critical heat flux and turbulent mixing in hexagonal tight rod bundles", International Journal of Multiphase Flow, Vol. 24, Iss. 8, 1998, pp. 1245-1263.